Nanoscale

PAPER

View Article Online
View Journal | View Issue

Cite this: *Nanoscale*, 2025, **17**, 12929

Engineering hydrophobic and electrostatic interactions for selective inactivation of bacteriophages by mixed-ligand nanoparticles†

Sada Raza, *[a] Pumza Mente,[a] Bartosz Kamiński,[a] Bartłomiej Bończak,[a] Hossein Maleki-Ghaleh,[a] Visesh Vignesh[b] and Jan Paczesny *[a]

Bacteriophage contamination poses significant challenges in bacteria-based industries, disrupting processes that rely on bacterial metabolism, such as insulin production using *Escherichia coli*. This study introduces mixed-ligand nanoparticles (MLNPs) as a novel solution for selective phage inactivation while preserving bacterial viability. By controlling the ratios of positively charged ((11-Mercaptoundecyl)-*N*,*N*,*N*-trimethylammonium cation, TMA), negatively charged (mercaptoundecanate anion, MUA), and hydrophobic (dodecane-1-thiol, DDT) ligands, MLNPs leverage tailored multivalent interactions to disrupt bacteriophage functions. The optimum MLNP formulation (60 : 20 : 18 ratio of TMA : MUA : DDT) achieved complete phage inactivation (7 log reduction) within 9 hours at 25 °C, a significant improvement over traditional methods that require harsh conditions, elevated temperatures, and/or extended durations. Our results demonstrate that hydrophobic ligands enhance phage inactivation while maintaining bacterial viability, with survival rates exceeding 90%. The MLNPs were tested against diverse bacteriophages, including MS2, M13, Qβ, LR1_PA01, and vB_SauS_CS1, achieving broad-spectrum efficacy without significant harm to host bacteria. Furthermore, cytotoxicity tests on mammalian 3T3 NIH fibroblast cells confirmed the high biocompatibility of MLNPs, with cell viability exceeding 90% at effective concentrations. This study highlights the potential of MLNPs as a selective and cost-effective tool for managing bacteriophage contamination, offering advantages for industrial and medical applications by ensuring bacterial productivity while mitigating phage-induced disruptions.

Received 11th February 2025,
Accepted 21st April 2025

DOI: 10.1039/d5nr00612k

rsc.li/nanoscale

Introduction

Bacteriophage contaminations pose a severe and persistent challenge in bacteria-based industries. Despite a plethora of well-known and broadly used disinfection strategies, phage infections routinely lead to significant economic losses by product spoilage and production line disruptions. This issue is of particular importance in critical biomedical bacterial products such as insulin, where *Escherichia coli* is routinely used for hormone production.[1]

Phage contaminations occur due to various factors such as the external introduction of phages, carryover from previously contaminated processes, and sources like raw materials, recycled ingredients, and unsterilized air/surfaces within the production environment.[2,3] Existing strategies to combat phage contamination include good laboratory practices, strict factory hygiene, sterilization, and disinfection using chemicals like Virkon (1%), sodium hypochlorite (2500 ppm available chlorine), and ethanol (75%).[4] Physical methods such as elevated temperatures,[5] UV radiation,[6] and high-pressure treatments are also employed.[7,8] However, despite advancements in these preventive and disinfectant approaches, the total effectiveness of phage infection treatments was inconsistent and varied due to factors such as phage resistance.[9]

The poor reliability of existing techniques necessitates reevaluating current strategies and exploring novel approaches to effectively and consistently mitigate phage contamination in bacteria-based factories. Nanoparticles like silver and gold have shown promise in antimicrobial applications,[10,11] but their effectiveness against phages and potential side effects remain uninvestigated.[12,13]

Nanoparticles with mixed ligand shells can selectively interact with either bacteriophages or bacteria due to the

[a]*Institute of Physical Chemistry, Polish Academy of Sciences, Kasprzaka 44/52, 01-224 Warsaw, Poland. E-mail: jpaczesny@ichf.edu.pl, sraza@ichf.edu.pl; Tel: +48 22 343 2071*
[b]*Department of Chemical Engineering and Centre for Bioengineering and Biomedical Technologies (CBio), University of Bath, BA2 7AY Bath, UK*
† Electronic supplementary information (ESI) available. See DOI: https://doi.org/10.1039/d5nr00612k

multivalent interactions arising from the varied ligand ratios.[13] These multivalent interactions significantly enhance the specificity and strength of target binding.[14] Particular combinations of these interactions match the diverse molecular constituents of virions or bacterial cell envelopes, mimicking "lock and key" type selectivity. The mixed ligand shell on the nanoparticles allows for a customizable and precise arrangement of functional groups that can simultaneously engage multiple binding sites on the target surface.[15] Adjusting the ratios and types of ligands on the nanoparticles makes it possible to fine-tune the binding affinity and target either phages or bacteria. This approach leverages the unique molecular surface mosaics present on the target to achieve the desired specificity, independent of site-specific domains or labels.[13] Grzybowski *et al.*[15] demonstrated a Gram-selective antibacterial action using mixed ligand gold nanoparticles. Their experiments showcased how varying proportions of positively and negatively charged ligands ((11-mercaptoundecyl)-*N*,*N*,*N*-trimethylammonium bromide, TMA, and mercaptoundecanoic acid, MUA, respectively) functionalized on gold nanoparticles led to the disruption of bacterial cell walls. This approach highlighted the potential of mixed charge nanoparticles in targeting specific types of bacteria, paving the way for selective antimicrobial strategies.[15] Furthermore, the Stellacci group investigated the influence of ligand density and particle size on antiviral efficacy,[16] demonstrating that the inhibitory concentration (IC50) depended on ligand concentration of silica nanoparticles modified with negatively charged 11-mercapto 1-undecanesulfonic acid (MUS).

Our recent study on mixed-ligand gold nanoparticles identified hydrophobicity as a key factor in promoting effective phage deactivation through surface interactions.[13] Gold nanoparticles coated with MUS were unable to inactivate phages, but upon the addition of hydrophobic 1-octanethiol (OT) ligands, phages were irreversibly distorted.[13]

This study presents a targeted approach to phage inactivation based on tailored interactions between nanoparticles and surface ligand mosaics on phages. The strategy involves leveraging – custom engineered electrostatic and hydrophobic interactions for selective phage inactivation, offering key advantages over existing methods, such as good bacterial cell viability, eliminating the need for extreme physical and/or toxic reagent treatments, and significant customizability for different phage species. Gold nanoparticles were synthesized and functionalized with three types of ligands – (TMA, positive charge), mercaptoundecanoic acid (MUA, negative charge), and dodecane-1-thiol (DDT, hydrophobic) – to generate nanoparticles with varied surface characteristics. Nanoparticles were analyzed using nuclear magnetic resonance (NMR), scanning transmission electron microscopy (STEM), dynamic light scanning (DLS), and zeta potential measurements. The biological behavior of the nanoparticles against bacteriophages T4, MS2, M13, Qβ, P22, LR1_PA01, and vs_SauS_CS1 and their bacterial hosts *E. coli* BL21, *E. coli* C3000, *Pseudomonas aeruginosa* PAO1, and *Staphylococcus aureus* DSM10252 was evaluated at different time points and concentrations. Cytotoxicity tests were evaluated using 3T3 NIH fibroblast cells through AlamarBlue assay.

Bacteriophages can serve as models for pathogenic viruses that infect complex organisms, including humans (*e.g.*, Phi6,[17] phiX174,[18] and MS2 [19]). The approach presented here could represent a significant step in preventing disease transmission by inactivating virions before they cause infections. Unlike most current treatments that target host cells to block viral replication,[20] MLNPs offer a more direct strategy by acting on the viruses themselves, offering a high degree of biocompatibility.

Materials and methods

Synthesis of nanoparticles

Chemicals. Didodecyldimethylammonium bromide (DDAB) (>98%) was purchased from TCI, Japan. Tetrabutylammonium borohydride (98%), gold(III) chloride trihydrate (>99%), dodecyl amine (DDA) (98%), tetramethylammonium hydroxide (25% in water), mercaptoundecanoic acid (MUA) and dodecanethiol (DDT) were purchased from Sigma-Aldrich and used as received. Hydrazine hydrate (50%) was purchased from Sigma-Aldrich and distilled over KOH under an argon atmosphere to prepare anhydrous hydrazine, which was later stored under argon in the refrigerator. Toluene, chloroform, and methanol were purchased from Linegal Chemicals, Poland, and used without further purification. (11-Mercaptoundecyl)-*N*,*N*,*N*-trimethylammonium bromide (TMA) was synthesized according to a published procedure.[21]

Methods. DDA-capped Au nanoparticles in toluene were synthesized using a method previously reported by Jana and Peng,[22] using $HAuCl_4{\cdot}3H_2O$ instead of $AuCl_3$. The mixed ligand nanoparticles (MLNPs) were functionalized with TMA : MUA : DDT ratios of 0 : 100 : 0, 35 : 65 : 0, 43 : 57 : 0, 56 : 44 : 0, 75 : 25 : 0, 86 : 14 : 0, 60 : 22 : 18 and 0 : 100 : 0. To prepare the MLNPs, 45 mL 7.5 mM solution of DDA capped Au nanoparticles was quenched in methanol (120 mL) and the precipitate washed 3 times with methanol (40 mL) to remove any unreacted Au salt and excess DDT. The dried precipitate was re-dispersed in 45 mL toluene (or chloroform in the case of 43 : 57 : 0, 56 : 44 : 0, and 75 : 25 : 0) and divided into 5 mL aliquots. Functionalization was carried out by adding 2.5 mL of premixed chloroform solutions of the ligands to the toluene or chloroform solution of the nanoparticles. The solutions were left to mix overnight in an Orbi-Shaker at 400 rpm and then purified by washing with chloroform and acetone. The purified samples were allowed to dry and then re-dispersed in water to prepare 1 mg mL^{-1} solutions of MLNPs. Total thiol ligands were maintained at a constant level across all experiments by adding a 1 : 1 ligand : Au molar ratio. The carboxylic acid group of the MUA ligand was deprotonated by adding tetramethylammonium hydroxide before characterization and further use.

Characterization

Dynamic light scattering. The hydrodynamic size of the MLNPs was determined using the dynamic light scattering technique (DLS) with a Malvern ZetaSizer Nano-ZS instrument equipped with a DLS module (He–Ne lase 633 nm, max 4 mW). The MLNPs were diluted to 0.2 mg mL^{-1} in water containing tetramethylammonium hydroxide for deprotonating MUA ligands.

Zeta potential. The electrophoretic mobility of NPs was measured with Malvern ZetaSizer Nano-ZS, using Malvern disposable folded capillary cells. Before characterization, the MLNPs were diluted to 0.2 mg mL^{-1} in water containing 25 μL of 2% tetramethylammonium hydroxide for deprotonating MUA ligands.

UV-Vis. UV-Vis absorption spectra were recorded with a Thermo Scientific Evolution 220 spectrometer using 10 mm quartz cuvettes over the 400–750 nm range.

Scanning transmission electron microscopy (STEM) analysis. Measurements were carried out with FEI Nova NanoSEM 450 equipped with STEM II detector using 30 kV accelerating voltage in bright field mode (for size distribution curve) and high angle annular dark field mode (HAADF) for visualization of bacteriophage-nanoparticles interactions. The samples were diluted to 0.1 mg mL^{-1}, and 10 μL was drop-casted on lacy-carbon copper grids. The grids were allowed to dry sufficiently before TEM analysis.

Nuclear magnetic resonance (NMR). Proton NMR spectra were recorded with a Bruker (400 MHz) spectrometer. MLNPs were dried by rota-evaporation, re-dissolved in a methanol solution of iodine, and allowed to stand for 30 minutes to ensure the ligands were etched out of the Au surface. Afterward, the mixture was dried by rota-evaporation at 65 °C and left under vacuum overnight to ensure complete solvent removal. The dried samples were then dissolved in dry deuterated DMSO under Ar and immediately analyzed by NMR. An excess amount of iodide was added in some of the samples to downshift the residual water signal from 3.33 ppm, which overlapped with the TMA signal at 3.24 ppm.

Biological assessments

Chemicals. LB medium and LB-agar – 10 g L^{-1} of NaCl, 10 g L^{-1} of tryptone, and 5 g L^{-1} of yeast extract. For LB-agar, 15 g L^{-1} of agar was added to the LB medium. The media were ordered from Carl Roth (Germany). TM buffer (pH 7.4) was prepared by mixing 10 mM Tris base, 5 μM $CaCl_2$, 10 mM $MgSO_4$, and deionized water (MiliQ water purification system).

Consumables. 50 mL sterile falcon tubes (NeoCulture centrifuge tubes, made of PP, 50 mL, self-standing, sterile) and phage-safe 1.5 mL Eppendorf-type tubes (B-1429 and B-2278)[23] were purchased from Bionovo (Poland). Specific consumables that prevent virion adsorption on their inner surface were chosen.[24]

Bacteriophages. T4 (*Tevenviridae*), MS2 (*Leviviridae*), and M13 (*Inoviridae*) phages were purchased from Phage Consultants (Poland). QBeta (*Fiersiviridae*), P22 (*Lederbergvirus*), and vB_SauS_CS1 (*Siphovirus*) phages and their specific hosts were purchased from DSMZ (Germany). LR1_PA01 was isolated from the environment. It is a tailed phage isolated from the Baltic seawater (probably *Pbunavirus*). MS2 and QBeta, both icosahedral tailless bacteriophages, were selected due to their similarity with eukaryote-infecting viruses.[25,26] P22, known for its remarkable resilience,[27] and M13, a filamentous bacteriophage frequently utilized in nanotechnology applications,[28] were also included in the study. For Gram-positive bacteria phages, we chose vB_SauS_CS1, with *Staphylococcus aureus* as its host, to represent this category. Additionally, LR1_PA01, a tailed phage isolated from the environment with *Pseudomonas aeruginosa* as its host, was included.

Bacteria. The *E. coli* strain BL21 (obtained from the Institute of Biochemistry and Biophysics in Warsaw, Poland) was used as the host for the T4 phage. For MS2, M13 phages, and QBeta, the *E. coli* C3000 strain (obtained from the Institute of Biochemistry and Biophysics in Warsaw, Poland) was used. For LR1_PA01, we used *Pseudomonas aeruginosa* PAO1 strain (IChF PAN collection), while for P22 – *Salmonella enterica* DSM18522 (DSMZ, Germany), and for vB_SauS_CS1 – *Staphylococcus aureus* DSM10252 (DSMZ, Germany).

A single colony of the required strain was picked up from the stock plate and transferred to 10 mL of LB medium to prepare the bacterial cultures. This sample was then incubated overnight at 37 °C in the shaker (Orbital Shaker-Incubator ES-20, 200 rpm). The sample was refreshed by mixing 2.5 mL of the overnight culture with 7.5 mL of LB medium and incubating at 37 °C for approximately 1 h.

Double overlay titration for phage analysis. LB-agar medium (20 mL) was poured into Petri plates and left to solidify. 4 mL of top LB agar (prepared with liquid medium and 0.5% agar instead of 1.5% agar) was then mixed with 200 μL of the refreshed bacterial culture (of appropriate strain) and poured onto the plate. Dilutions of the phage solutions were prepared, and from each dilution, eight droplets of 5 μL solution were spotted onto the top agar layer. After incubation of the plates at 37 °C for 24 h, the number of plaques was counted. All titrations were performed in triplicate. Statisical significance was evaluated using a Student's *t*-test was performed. $*P < 0.05$; $**P < 0.01$; $***P < 0.001$.

Dosage compensation. Previous research reported that gold nanoparticles with only positively charged ligands possessed maximum antimicrobial efficacy. Therefore, we chose 100% TMA gold nanoparticles (100 : 0 : 0) to set the standard for the optimal concentration of nanoparticles that would be applied for all future experiments.

Duration of exposure. T4 bacteriophages were tested against nanoparticles functionalized with 100% TMA at a concentration of 0.1 mg mL^{-1}. Survival percentage was monitored hourly, up to 12 hours, to determine time-of-action of the TMA nanoparticles on bacteriophages.

Biocompatibility assay. The biocompatibility of modified gold nanoparticles was assessed using the Alamar Blue assay using 3T3 NIH fibroblast cells (Merck). All reagents were

obtained from commercial suppliers: Alamar Blue reagent (Thermo Fisher Scientific), Triton X-100 (Sigma-Aldrich), and Trypan Blue (Thermo Fisher Scientific). 3T3 NIH fibroblast cells were cultured in Dulbecco's Modified Eagle's medium (DMEM) supplemented with 10% fetal bovine serum (FBS) and 1% penicillin–streptomycin, in a humidified atmosphere at 37 °C and 5% CO_2. Cells were subcultured upon reaching 70–80% confluency and harvested for experiments during the log phase of growth. Cells were harvested and counted using Trypan Blue exclusion to ensure viable cell counts. Cells were diluted to a concentration of 7.5 × 104 cells per mL, and 200 μL of cell suspension (equivalent to 1.5 × 104 cells) was seeded into each well of a 96-well tissue culture-treated plate. The cells were incubated overnight at 37 °C with 5% CO_2 to allow for surface attachment.

Cells were treated with the nanoparticles at a 0.1 mg mL^{-1} concentration the following day. The cells were incubated with the nanoparticles for 24 and 48 hours at 37 °C in a humidified atmosphere with 5% CO_2. After each incubation period, the medium was aspirated and replaced with fresh medium containing 10% (v/v) Alamar Blue solution. The cells were incubated with the Alamar Blue mixture for 4 hours at 37 °C with 5% CO_2. After incubation, 150 μL of the medium from each well was transferred to a new 96-well plate, and fluorescence was measured using a plate reader with excitation at 530–570 nm and emission at 580–620 nm. The blank value (from wells without cells) was subtracted from each reading to ensure accuracy. Cell viability was calculated based on metabolic activity, which was directly proportional to the Alamar Blue fluorescence intensity.

Results and discussion

Characterization of MLNPs

The STEM image of gold nanoparticles before the ligand exchange reaction showed spherical nanoparticles with an average diameter of 11.6 ± 2.9 nm and a monodisperse size distribution (Fig. 1). This well-defined structure indicated successful synthesis, with the average size aligning with previous reports on gold nanoparticles used in antimicrobial studies.[22] The narrow size distribution suggested high reproducibility, essential for uniform behavior during ligand exchange and functionalization.[29] This size range was optimal for entering biological systems without triggering excessive immune responses,[30] and the spherical shape facilitated consistent interaction with bacterial surfaces and phages, which was crucial for selective bacteriophage inactivation.[13]

The proton NMR spectra of the modified nanoparticles (Fig. 2) revealed distinct signals corresponding to the different ligands attached to the gold nanoparticle surface. The peaks associated with MUA and TMA confirmed the successful functionalization of the nanoparticles. The spectrum of pure MUA in DMSO revealed overlapping of signals arising from CH_2COOH and SH groups, complicating the integration (Fig. 2(a)). However, when AuNPs were treated with iodine, the ligands detached from the gold surface, and sulfur atoms oxidized to form a disulfide bond.[31,32] As a result, the SH signal disappeared, and the methylene group signal next to the sulfur atom (–CH_2S–) shifted to 2.68 ppm.[33] In some spectra, a triplet at 2.17 ppm, attributed to the methylene group next to the deprotonated carboxyl group, was also observed. The integrals of these signals were combined to quantify the MUA ligands.[34] Signals at 3.24 ppm, corresponding to the CH_2 protons adjacent to the $N(CH_3)^+$ group in TMA (Fig. 2(b)), were often difficult to integrate due to the overlapping water peak at 3.33 ppm.[33] Therefore, the $N(CH_3)^+$ singlet at 3.02 ppm was used for quantifying the TMA ligand, with the integral ratio of 9 : 2 correlating with the 3.24 ppm signal, whenever possible (Fig. 2(b) and S1†).[35] The chemical shifts of relevant groups are provided in ESI in Table S1.† The NMR spectra for all the intermediary ratios can be found in ESI, Fig. S1.† The ability to control ligand ratios was crucial for fine-tuning nanoparticle surface properties, affecting their interaction with biological targets, and enabling selective bacteriophage inactivation while preserving bacterial viability.[15]

The hydrodynamic diameters of the MLNPs were determined using the DLS technique and are presented in Fig. 3(a).

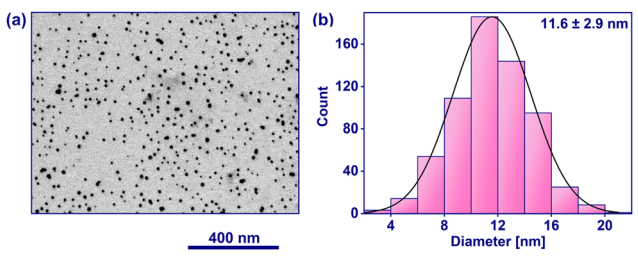

Fig. 1 STEM image and size distribution of gold nanoparticles before ligand exchange reaction. (a) Representative STEM image showing spherical gold nanoparticles with an average diameter of 11.6 ± 2.9 nm. (b) Size distribution based on STEM measurements.

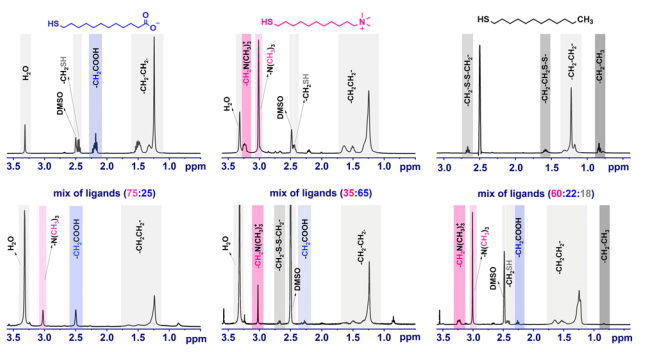

Fig. 2 NMR spectra of ligands before and after removal of gold nanoparticles *via* iodine (I_2). (a) NMR spectrum of pure MUA, (b) NMR spectrum of pure TMA, (c) NMR spectrum of dodecanethiol (DDT) oxidized with iodine, (d) NMR spectrum of a reaction mixture after I_2 oxidation with a 75 : 25 ratio of TMA : MUA, (e) NMR spectrum of a ligand mixture with a 35 : 65 ratio of TMA : MUA, and (f) NMR spectrum of a ligand mixture with a 60 : 22 : 18 ratio of TMA : MUA : DDT.

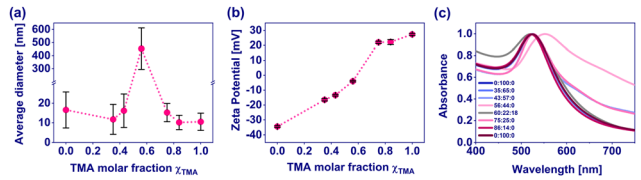

Fig. 3 (a) Dynamic light scattering size data and (b) zeta potential of the mixed ligand nanoparticles (MLNPs) where the core is gold nanoparticles and the ligands are positively charged (TMA), negatively charged (MUA), and hydrophobic (DDT) in nature. (c) UV-Vis analysis (0 : 100 : 00 and 35 : 65 : 0 and 100 : 0 : 0 and 86 : 14 : 0 is overlapping).

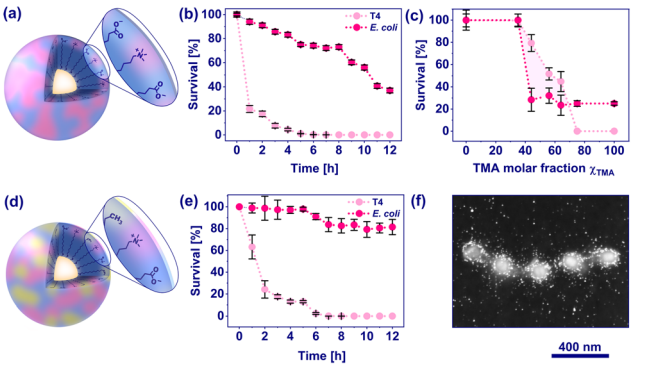

Fig. 4 (a) Schematic representation of mixed ligand nanoparticles functionalized with TMA and MUA. (b) Fluctuations in survival percentage of T4 bacteriophages over time following exposure to all-TMA nanoparticles (100 : 0 : 0). The starting T4 concentration was 10^7 PFU mL^{-1} and nanoparticle concentration was 10^{-1} mg mL^{-1}. The experiment was carried out for 12 hours at 25 °C, 220 rpm, with readings taken every hour. (c) Survival percentage trends of T4 and *E. coli* treated with MLNPs. The shaded area between the plots shows the difference in survival percentages. The starting concentration of T4 was 10^7 PFU mL^{-1}, while that of *E. coli* was 10^5 CFU mL^{-1}. The experiment was conducted for 5 hours at 25 °C, 220 rpm. The concentration of nanoparticles was 10^{-1} mg mL^{-1}. (d) Schematic representation of mixed ligand nanoparticles functionalized with TMA, MUA, and DDT. (e) Effect of nanoparticles containing positive, negative, and hydrophobic ligands on the survivability of *E. coli* and T4. The starting concentration of *E. coli* was 10^5 CFU mL^{-1}, while that of T4 was 10^7 PFU mL^{-1}. The experiment was conducted for 5 hours at 25 °C, 220 rpm. The concentration of nanoparticles was 10^{-1} mg mL^{-1}. (f) STEM visualization of T4 bacteriophages in the presence of hydrophobic mixed ligand nanoparticles after 5 hours of incubation at 25 °C, 220 rpm [Scale set to 400 nm].

DLS analysis showed that mixed-ligand nanoparticles (MLNPs) with a near-equal ratio of positive (TMA) and negative (MUA) ligands (56 : 44 : 0) formed large aggregates (~450 nm), indicating reduced stability due to decreased electrostatic repulsion.[36] In contrast, nanoparticles with purely positive (100 : 0 : 0) or negative (0 : 100 : 0) ligands exhibited smaller, more stable hydrodynamic diameters. This was further supported by zeta potential measurements (Fig. 3(b)), where TMA-functionalized particles had a positive charge (+29 mV), MUA-functionalized particles had a negative charge (−35 mV), and mixed-ligand particles had reduced zeta potentials, approaching neutrality, leading to aggregation.[13] Zeta potential from around −10 mV to +10 mV is usually associated with unstable colloidal suspension, where electrostatic repulsion is insufficient to prevent aggregation.[37]

UV-Vis absorption spectra (Fig. 3(c)) showed that purely positive MLNPs had a peak at 522 nm, while negative MLNPs exhibited a slight shift to 525 nm. The intermediate ligand ratio (56 : 44 : 0) displayed a red-shifted peak around 560 nm, further indicating particle aggregation.[29,38–40] Some aggregation also occurred in (43 : 57 : 0) and (75 : 25 : 0) samples, where a long-wavelength tail was observed. The extent of this was relatively small, as aggregates were not visible in DLS. These results underscore the importance of controlling ligand ratios to maintain nanoparticle stability, which is critical for applications such as selective bacteriophage inactivation.[32]

Antiphage and antibacterial efficacy

Concentrations of MLNPs ranging from 10^{-7} up to 1 mg mL^{-1} were tested, and double overlay titration was carried out to attain the extent of phage inactivation of T4 bacteriophages. The dosage compensation experiment established that a 0.1 mg mL^{-1} concentration of MLNPs was sufficient to deactivate over 90% of T4 bacteriophages after 3 hours at 25 °C (Fig. S2, ESI†). These values show a strong positive correlation with our previous research.[13]

Observing the phage-nanoparticle mixture over time demonstrated that TMA-functionalized nanoparticles (100 : 0 : 0) inactivated over 99% of T4 bacteriophages within 5 hours at a concentration of 0.1 mg mL^{-1} while maintaining approximately 80% *E. coli* viability (Fig. 4(b)).

The nanoparticles were tested against T4 and *E. coli* as model organisms for bacteriophages and bacteria. The virions and bacterial cells were individually exposed to each set of nanoparticles, and any changes in their respective concentrations were recorded. It was observed that nanoparticles with a higher amount of positive ligands (TMA) inactivated both phages and bacteria. In contrast, nanoparticles with a higher ratio of negative ligands had little to no effect on either phage titer or bacterial cell concentration. The shaded area between the plots in Fig. 4(c) shows the difference in survival percentages of *E. coli* and T4 bacteriophages, where MLNPs were more efficient against virions than bacterial cells, *i.e.*, ligand ratios allowing for selectivity.

The nanoparticles were further modified by adding a hydrophobic ligand (dodecanethiol, DDT), as shown in Fig. 4(d), to obtain nanoparticles with a 60 : 22 : 18 ratio of TMA : MUA : DDT. Previous research showed that introducing hydrophobic ligands to all-negative NPs increased the efficacy of phage inactivation.[13] However, those nanoparticles (0 : 85 : 15) were only efficient inactivators at 50 °C and with prolonged exposure times. Here, we aimed to achieve phage eradication at 25 °C and at a shorter time scale, and thus, a mixture of three different ligands (TMA : MUA : DDT) was tested. Such hy-MLNPs were tested against both *E. coli* and T4 bacteriophages to assess their impact on bacterial cell viability and phage titer. After 5 hours, approximately 87% of T4 phages were inactivated, while 90% of all bacterial cells survived (Fig. 4(e)). These findings highlight the potential of the

tested nanoparticles as effective agents against bacteriophages while simultaneously preserving bacterial cell viability.

STEM images obtained subsequent to a 5-hour incubation period of T4 bacteriophages with hy-MLNPs demonstrated an apparent interaction between nanoparticles and the capsids of T4 phages (Fig. 4(f)). Other research has shown the interaction between phage capsids and gold nanoparticles by forming an amide bond between the terminal carboxylic groups on ligands and amine groups on phage capsids.[41]

In this work, it was observed that nanoparticles encircled the T4 phage capsids, likely causing them to cluster in chain-like formations. Such interactions were previously observed when we performed TEM analysis of modified gold nanoparticles (with hydrophobic ligands) with T4 phages.[13]

Based on the experiments in this study, we propose two possible mechanisms of action for MLNP inactivation of bacteriophages.

The first proposed mechanism of action for MLNPs involves the disruption of electrostatic interactions at the target surface. Upon approaching the surface, the high surface charge of the MLNPs alters the local charge environment, reducing ionic strength and shortening the Debye length, which controls the range of electrostatic forces.[29] This disruption weakens the interactions that maintain the structural integrity of virions, which is in agreement with the findings of Wennerström *et al.*, who emphasized the critical role of electrostatic interactions in colloidal stability.[42]

The second mechanism relates to osmotic pressure changes induced by the high charge density of the MLNPs and their counter ions. This creates a localized osmotic imbalance,[43] leading to water influx near the virions. Virions are particularly susceptible to such osmotic fluctuations due to the high internal pressure within their capsid, resulting from the tightly packed genetic material.[44] The increased osmotic stress may compromise capsid integrity, further inhibiting the virion's functionality.[44]

Hydrophobic mixed ligand nanoparticles against other model phages

After demonstrating high effectiveness *versus* T4 bacteriophages, the hy-MLNP with a 60 : 22 : 18 ratio of TMA : MUA : DDT was tested against several model bacteriophages, including MS2, M13, Qβ, LR1_PA01, and vB_SauS_CS1 (Fig. 5). The nanoparticles achieved complete inactivation (100%, 7 log reduction) of all phages within 9 hours. A comparison between the phages and their corresponding bacterial strains is shown in Fig. 5. M13 exhibited the most rapid inactivation, with approximately 91% inactivation within just 3 hours (Fig. 5). Following closely were LR1_PAO1 and MS2, demonstrating around 95% inactivation after 5 hours of exposure to the nanoparticles. vB_SauS_CS1 was fully inactivated after 8 hours, although it required longer incubation than the aforementioned phages. These results demonstrate the broad-spectrum efficacy of the mixed-ligand nanoparticles in inactivating a wide range of bacteriophages, suggesting that the combination of TMA, MUA, and DDT ligands is effective against various phage structures. It must be emphasized that

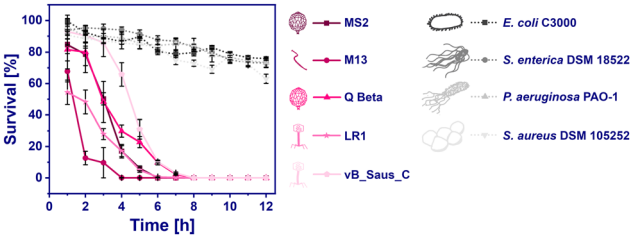

Fig. 5 Impact of nanoparticles on the survivability of diverse model phages (MS2, M13, Q Beta, LR1_PA01, and vB_SauS_CS1) and bacterial host species, quantifying their inactivation over 12 hours. Initial phage titer: 10^7 PFU mL^{-1}, initial bacterial concentration: 10^5 CFU mL^{-1}. Experiments were conducted at 25 °C, 220 rpm, with nanoparticle concentration at 0.1 mg mL^{-1}.

previously reported (0 : 85 : 15) particles were not active against MS2 even at elevated temperatures.[13] This underlines the importance of multivalent interactions and proper design of the nano-objects to tailor their properties specifically to a particular application.

Interestingly, the nanoparticles were able to combine strong antiviral action with high selectivity for phages. Even at the exposure time required for maximum phage inactivation (7 log), bacterial cell viability was maintained between 70–80%. The viability tests held true for all host bacteria species tested (*E. coli* BL21, *E. coli* C3000, *Pseudomonas aeruginosa* PAO1, *Salmonella enterica* DSM18522, and *Staphylococcus aureus* DSM10252). This selective targeting of phages makes the nanoparticles highly suitable for applications in industries where bacteriophage contamination must be controlled without compromising the productivity of beneficial bacterial cultures.[13]

Previous research has demonstrated that fine-tuning surface chemistry can effectively differentiate Gram-negative from Gram-positive bacteria.[15] Our study extended this concept by successfully distinguishing bacteriophages from bacterial cells based on their surface characteristics.

Biocompatibility assay

To evaluate the biocompatibility of our nanoparticles on mammalian cells, an Alamar Blue assay was conducted using the 3T3 NIH fibroblast cell line. Three types of nanoparticles were tested: gold nanoparticles before ligand exchange reaction (AuNPs), mixed ligand nanoparticles (56 : 44 : 0 ratio of TMA and MUA), and mixed ligand nanoparticles incorporating a hydrophobic ligand (60 : 22 : 18 ratio of TMA : MUA : DDT). The chosen concentration was 0.1 mg mL^{-1}, based on its effective performance in phage inactivation assays (Fig. S2†).

3T3 NIH cells were treated with different nanoparticle formulations, including AuNPs, MLNPs (56 : 44 : 0), and MLNPs (60 : 22 : 18), for 24 and 48 hours. Cell viability was assessed using the Alamar Blue assay, which measured the conversion of resazurin to its fluorescent product, resorufin. The quantitative results in Fig. 6(f) demonstrate that cell viability exceeded 90% for all nanoparticle types at both time points. This indicated minimal cytotoxicity at the tested concen-

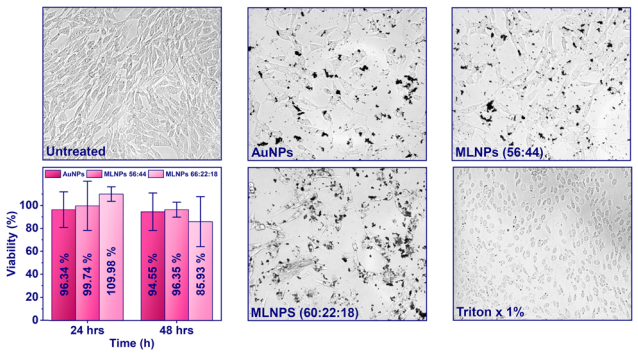

Fig. 6 Optical microscopic images of 3T3 NIH fibroblast cells after 24 hours of incubation with different nanoparticle treatments: (a) untreated control cells, (b) cells treated with gold nanoparticles (AuNPs, 0.1 mg mL^{-1}), (c) cells treated with mixed ligand nanoparticles (MLNPs, 56 : 44 TMA : MUA, 0.1 mg mL^{-1}), (d) viability of cells treated with AuNPs, MLNPs (56 : 44), and MLNPs (60 : 22 : 18) after 24 and 48 hours of incubation. (e) Cells treated with MLNPs (60 : 22 : 18 TMA : MUA : DDT, 0.1 mg mL^{-1}) and (f) cells treated with 1% Triton X.

trations, with particularly high viability observed for MLNPs (56 : 44 : 0).

Observations of cell morphology further confirmed nanoparticle biocompatibility. Untreated control cells (Fig. 6(a)) maintained their characteristic elongated, spindle-like morphology, typical of healthy 3T3 fibroblasts. Similarly, cells exposed to gold nanoparticles before ligand exchange reaction (AuNPs; Fig. 6(b)) and MLNPs with positive and negative ligands (56 : 44, TMA : MUA; Fig. 6(c)) displayed no significant morphological changes compared to controls. Cells treated with MLNPs incorporating hydrophobic ligands, hy-MLNP (60 : 22 : 18, TMA : MUA : DDT; Fig. 6(d)), exhibited slightly higher nanoparticle interaction but retained their fibroblast morphology. In contrast, cells treated with Triton X-100 (1%; Fig. 6(e)), *i.e.*, negative control, showed spherical, shrunken morphologies indicative of cell death, confirming the assay's sensitivity in detecting cytotoxic effects.

These results suggest that both MLNPs and hy-MLNPs retain high biocompatibility with 3T3 NIH cells, with cell viability consistently above 90%. This high selectivity index, demonstrated by effective phage inactivation alongside minimal cytotoxicity, highlights the potential of these nanoparticles for applications in medical and antimicrobial settings, where selective phage inactivation is required without adverse effects on mammalian cells. These findings align with prior research, indicating that ligand-functionalized nanoparticles, particularly those with carboxyl or hydrophobic functionalities, enhance biocompatibility and selectively target microbial contaminants without harming mammalian cells.[45]

Conclusions

This study demonstrates the potential of two-component mixed-charged nanoparticles and three-component (with the addition of hydrophobic ligands, hy-MLNPs) nanoparticles for targeted bacteriophage inactivation in bacteria-based industries. Phage contamination remains a critical challenge across pharmaceuticals, biotechnology, and agriculture sectors, often resulting in severe economic and operational losses. By tuning nanoparticle functionalization with positive, negative, and hydrophobic ligands, this work demonstrates a robust and selective approach to phage inactivation while preserving bacterial viability.

Our results underscore the significance of precise ligand ratio tuning, with the hy-MLNPs (60 : 22 : 18 ratio of TMA : MUA : DDT) achieving complete phage inactivation (7 log reduction) within 9 hours at 25 °C against a plethora of phages (T4, MS2, M13, Qβ, LR1_PA01, and vB_SauS_CS1). This represents a notable advancement compared to traditional methods, which often require elevated temperatures or longer treatment duration. Moreover, introducing hydrophobic ligands enhances phage inactivation efficiency without compromising bacterial viability. Additionally, post-treatment bacterial survival rates were high, with a survival rate of 70% to 80% after around 9 hours of incubation. This is crucial for biotechnological applications, where bacteria are used to produce active compounds, *e.g.*, drugs.

The proposed combination of electrostatic and hydrophobic interactions ensures specificity in targeting bacteriophages while maintaining minimal cytotoxicity, as confirmed by mammalian cell studies. The cytotoxicity assay on 3T3 NIH fibroblasts demonstrated over 90% cell viability for all tested nanoparticle formulations, emphasizing their high biocompatibility and potential suitability for medical and antimicrobial applications.

Future research should focus on optimizing MLNP formulations to ensure scalability, cost-effectiveness, and safety for industrial applications. Integrating these nanoparticles into existing bioprocessing workflows could provide a sustainable solution to mitigate phage contamination, safeguarding product quality and enhancing the efficiency of bacteria-based industries.

Data availability

Data for this article, including raw data for all performed experiments, are available at RepOD at **https://doi.org/10.18150/WMSQQI**.

Conflicts of interest

There are no conflicts to declare.

Acknowledgements

The research was financed by the National Science Centre, Poland, within the OPUS grant number 2022/45/B/ST5/01500. We acknowledge Witold Adamkiewicz for his help with STEM visualization.

References

1 N. A. Baeshen, M. N. Baeshen, A. Sheikh, R. S. Bora, M. M. M. Ahmed, H. A. I. Ramadan, K. S. Saini and E. M. Redwan, *Microb. Cell Fact.*, 2014, **13**, 1–9.

2 M. Łoś, *Open J. Bacteriol.*, 2020, **4**, 020–023.

3 J. E. Garneau and S. Moineau, *Microb. Cell Fact.*, 2011, **10**, 1–10.

4 D. E. Halfhide, B. W. Gannon, C. M. Hayes and J. M. Roe, *Lett. Appl. Microbiol.*, 2008, **47**, 608–612.

5 M. Blazanin, W. T. Lam, E. Vasen, B. K. Chan and P. E. Turner, *PLoS One*, 2022, **17**, 1–13.

6 D. K. Kim, S. J. Kim and D. H. Kang, *Food Res. Int.*, 2017, **91**, 115–123.

7 O. Moroni, J. Jean, J. Autret and I. Fliss, *Int. Dairy J.*, 2002, **12**, 907–913.

8 N. Komora, C. Bruschi, V. Ferreira, C. Maciel, T. R. S. Brandão, R. Fernandes, J. A. Saraiva, S. M. Castro and P. Teixeira, *Food Microbiol.*, 2018, **76**, 416–425.

9 S. P. M. B. Marcó, V. B. Suárez and A. Quiberoni, *Viruses*, 2019, **11**, 1–28.

10 H. Choudhury, M. Pandey, Y. Q. Lim, C. Y. Low, C. T. Lee, T. C. L. Marilyn, H. S. Loh, Y. P. Lim, C. F. Lee, S. K. Bhattamishra, P. Kesharwani and B. Gorain, *Mater. Sci. Eng., C*, 2020, **112**, 110925.

11 A. Shome, S. Dutta, S. Maiti and P. K. Das, *Soft Matter*, 2011, **7**, 3011–3022.

12 V. Cagno, M. Gasbarri, C. Medaglia, D. Gomes, S. Clement, F. Stellacci and C. Tapparel, *Antimicrob. Agents Chemother.*, 2020, **64**, 1–8.

13 Ł. Richter, K. Paszkowska, U. Cendrowska, F. Olgiati, P. J. Silva, M. Gasbarri, Z. P. Guven, J. Paczesny and F. Stellacci, *Nanoscale*, 2021, **13**, 18684–18694.

14 F. Karush, *Contemp. Top. Mol. Immunol.*, 1976, **1937**, 217–228.

15 P. P. Pillai, B. Kowalczyk, K. Kandere-Grzybowska, M. Borkowska and B. A. Grzybowski, *Angew. Chem., Int. Ed.*, 2016, **55**, 8610–8614.

16 H. Wang, X. Xu, R. La Polla, P. J. Silva, Q. K. Ong and F. Stellacci, *J. Colloid Interface Sci.*, 2024, **657**, 327–333.

17 G. M. String, M. R. White, D. M. Gute, E. Mühlberger and D. S. Lantagne, *Environ. Sci. Technol. Lett.*, 2021, **8**(11), 995–1001.

18 R. Cheng, Y. Zhang, T. Zhang, F. Hou, X. Cao, L. Shi and P. Jiang, *Front. Environ. Sci. Eng.*, 2022, **16**, 108.

19 M. Shaffer, K. Huynh, V. Costantini, J. Vinjé and K. Bibby, *J. Appl. Microbiol.*, 2024, **135**(2), 1364–5072.

20 S. Raza, M. Wdowiak and J. Paczesny, *EcoSal Plus*, 2023, **11**, 0019–2022.

21 P. Thebault, E. Taffin de Givenchy, R. Levy, Y. Vandenberghe, F. Guittard and S. Géribaldi, *Eur. J. Med. Chem.*, 2009, **44**, 717–724.

22 N. R. Jana and X. Peng, *J. Am. Chem. Soc.*, 2003, **125**, 14280–14281.

23 Ł. Richter, K. Księżarczyk, K. Paszkowska, M. Janczuk-Richter, J. Niedziółka-Jönsson, J. Gapiński, M. Łoś, R. Hołyst and J. Paczesny, *Sci. Rep.*, 2021, **11**, 1–12.

24 K. Matuła, Ł. Richter, M. Janczuk-Richter, W. Nogala, M. Grzeszkowiak, B. Peplińska, S. Jurga, E. Wyroba, S. Suski, H. Bilski, A. Silesian, H. A. R. Bluyssen, N. Derebecka, J. Wesoły, J. M. Łoś, M. Łoś, P. Decewicz, L. Dziewit, J. Paczesny and R. Hołyst, *Sci. Rep.*, 2019, **9**, 1–12.

25 M. O. Mohsen, G. Augusto and M. F. Bachmann, *Immunol. Rev.*, 2020, **296**, 155–168.

26 R. Jain and R. Srivastava, *BMC Syst. Biol.*, 2009, **3**(121), 1–11.

27 L. Gildea, J. A. Ayariga, B. K. Robertson and R. Villafane, *Arch. Microbiol. Immunol.*, 2022, **6**, 81–100.

28 F. Fouladvand, P. Bemani, M. Mohammadi, R. Amini and F. A. Jalilian, *J. Appl. Biotechnol. Rep.*, 2020, **7**, 7–15.

29 P. P. Pillai, B. Kowalczyk and B. A. Grzybowski, *Nanoscale*, 2016, **8**, 157–161.

30 D. Wang, R. J. Nap, I. Lagzi, B. Kowalczyk, S. Han, B. A. Grzybowski and I. Szleifer, *J. Am. Chem. Soc.*, 2011, **133**, 2192–2197.

31 H. Häkkinen, *Nat. Chem.*, 2012, **4**, 443–455.

32 S. Engel, E. C. Fritz and B. J. Ravoo, *Chem. Soc. Rev.*, 2017, **46**, 2057–2075.

33 D. L. B. Robert, M. Silverstein, F. X. Webster and D. J. Kiemle, *Spectrometric Identification of Organic Compounds*, Wiley, 8th edn, 2014.

34 K. B. Dillon, M. R. Harrison and F. J. C. Rossotti, *J. Magn. Reson.*, 1980, **39**, 499–508.

35 M. S. Gruzdev, L. E. Shmukler, N. O. Kudryakova, A. M. Kolker and L. P. Safonova, *J. Mol. Liq.*, 2018, **249**, 825–830.

36 D. Wang, B. Kowalczyk, I. Lagzi and B. A. Grzybowski, *J. Phys. Chem. Lett.*, 2010, **1**, 1459–1462.

37 J. D. Clogston and A. K. Patri, *Methods Mol. Biol.*, 2011, **697**, 63–70.

38 H. J. Jang, S. H. R. Shin and H. Y. Lee, *J. Nanopart. Res.*, 2018, **20**(244), 1–12.

39 S. M. Ansar, S. Chakraborty and C. L. Kitchens, *Nanomaterials*, 2018, **8**, 1–12.

40 R. Pamies, J. G. H. Cifre, V. F. Espín, M. Collado-González, F. G. D. Baños and J. G. De La Torre, *J. Nanopart. Res.*, 2014, **16**(2376), 1–11.

41 N. Tawil, E. Sacher, E. Boulais, R. Mandeville and M. Meunier, *J. Phys. Chem. C*, 2013, **117**, 20656–20665.

42 H. Wennerström, E. V. Estrada, J. Danielsson and M. Oliveberg, *Proc. Natl. Acad. Sci. U. S. A.*, 2020, **117**, 10113–10121.

43 M. Deserno and H. H. von Grünberg, *Phys. Rev. E: Stat., Nonlinear, Soft Matter Phys.*, 2002, **66**, 11401.

44 W. M. Gelbart and C. M. Knobler, *Phys. Today*, 2008, **61**, 42–47.

45 P. Makvandi, S. Iftekhar, F. Pizzetti, A. Zarepour, E. N. Zare, M. Ashrafizadeh, T. Agarwal, V. V. T. Padil, R. Mohammadinejad, M. Sillanpaa, T. K. Maiti, G. Perale, A. Zarrabi and F. Rossi, *Environ. Chem. Lett.*, 2021, **19**, 583–611.